Molecular Design of Antifouling Polymer Brushes Using Sequence-Specific Peptoids

King Hang Aaron Lau, Tadas S. Sileika, Sung Hyun Park, Ana M. L. Sousa, Patrick Burch, Igal Szleifer, and Phillip B. Messersmith**

Material systems that can be used to flexibly and precisely define the chemical nature and molecular arrangement of a surface would be invaluable for the control of complex biointerfacial interactions. For example, progress in antifouling polymer biointerfaces that prevents nonspecific protein adsorption and cell attachment, which can significantly improve the performance of an array of biomedical and industrial applications, is hampered by a lack of chemical models to identify the molecular features conferring their properties. Poly(*N*-substituted glycine) "peptoids" are peptidomimetic polymers that can be conveniently synthesized with specific monomer sequences and chain lengths, and are presented as a versatile platform for investigating the molecular design of antifouling polymer brushes. Zwitterionic antifouling polymer brushes have captured significant recent attention, and a targeted library of zwitterionic peptoid brushes with different charge densities, hydration, separations between charged groups, chain lengths, and grafted chain densities, is quantitatively evaluated for their antifouling properties through a range of protein adsorption and cell attachment assays. Specific zwitterionic brush designs are found to give rise to distinct but subtle differences in properties. The results also point to the dominant roles of the grafted chain density and chain length in determining the performance of antifouling polymer brushes.

1. Introduction

Poly(*N*-substituted glycine) "peptoids" are structural isomers of peptides, with sidechain attachment shifted from the α-carbon to the amide nitrogens of the peptide backbone. Peptoid chemical properties are determined, like peptides, by the specific sequence order of different monomers arranged along the polymer chain. Originally developed as a peptidomimetic drug discovery platform, peptoids can be conveniently synthesized with monomer-by-monomer sidechain sequence and chain length control using "submonomer" solid-phase synthesis.[1,2] Diverse sidechains, including mimics of all natural amino acids, can be incorporated.[2,3] A wide range of therapeutics and protein binding sequences have been identified.[1,2,4] The synthetic versatility of peptoids has also enabled recent studies on controlling polymer chain conformation and nanostructure self-assembly by monomer sequence design.[1,5] These studies have led to nascent peptoid biomaterials applications.[6]

Surfaces displaying a wide range of chemical designs have been intensely investigated for preventing biofouling—the undesired, non-specific attachment of biomolecules, cells, and organisms.[7–9] Effective antifouling surfaces could improve the efficacy of biomedical devices, biosensors, and nanomedicine,[8,10,11] and reduce the high costs associated with biofouling on an array of industrial surfaces.[7,12] Different surface chemical properties, including surface hydration, electrostatic neutrality, and flexibility in molecular packing, have been shown to confer antifouling behavior.[8,9,11,13] However, their relative contributions are unclear and a general theoretical understanding is lacking. Additional steric and entropic hindrance to protein adsorption can be achieved by end-tethering water soluble polymers to form antifouling surface-grafted polymer brushes,[8,11,14] provided that the grafting density and chain length are suitably controlled.[15–17] Poly(ethylene glycol) (PEG) polymer brushes exhibit very good antifouling properties but are susceptible to oxidative degradation.[7,9] Novel antifouling designs are actively being pursued,[7,8,11] and a need exists for versatile and precise chemical models to correlate the molecular features conferring antifouling properties.[7]

Recent reports of zwitterionic antifouling surfaces have attracted great attention.[8,18] The remarkable resistance of zwit-

Dr. K. H. A. Lau,[+] Dr. T. S. Sileika, Dr. S. H. Park, Dr. P. Burch, Prof. I. Szleifer, Prof. P. B. Messersmith[++,+++]
Biomedical Engineering Department
Chemistry of Life Processes Institute
Northwestern University
Evanston, Illinois 60208, USA
E-mail: aaron.lau@strath.ac.uk; philm@berkeley.edu

A. M. L. Sousa
Department of Pure and Applied Chemistry
University of Strathclyde
Glasgow G1 1XL, UK

Prof. I. Szleifer
Department of Chemistry and Department of Chemical and Biological Engineering and the Robert H. Lurie Comprehensive Cancer Center
Northwestern University, Evanston, Illinois 60208, USA

[+]Present address: Department of Pure and Applied Chemistry, University of Strathclyde, Glasgow, G1 1XL, UK.
[++]Department of Materials Science and Engineering, Institute for Bionanotechnology in Medicine and Department of Chemical and Biological Engineering and the Robert H. Lurie Comprehensive Cancer Center, Northwestern University, Evanston, Illinois 60208, USA
[+++]Present address: Departments of Materials Science and Engineering and Bioengineering, University of California, Berkeley, California 94720, USA

DOI: 10.1002/admi.201400225

terionic surfaces against biofouling is frequently attributed to their high degrees of ionic hydration.[18,19] Zwitterionic mixed self-assembled monolayers (SAMs) and copolymers bearing a balanced number of positively and negatively charged monomers can be synthetically more convenient than betaine-bearing surfaces and often exhibit comparable antifouling properties.[8,18,19] Zwitterionic designs generally exhibit improved antifouling properties relative to surfaces bearing a net positive or negative charge[20–23]; however, an advantage over uncharged designs is not always observed.[20,24,25] Model studies employing mixed SAMs can be biased by nanophase separation[26] or the electrostatic pairing of opposite charges.[19,22] The antifouling properties of surface-grafted polymer models can be greatly influenced by polydispersity and grafted brush density,[23,27] which are not easily controlled especially for surface-initiated polymerization. The ratio of different monomers incorporated into the polymer may also differ from the copolymerization feed ratio.[23]

In this contribution, we exploit the precise sequence programmability of peptoids to investigate the antifouling properties of surface-grafted polymer brushes, especially in relation to zwitterionic designs. The peptoid system allowed us to conveniently prepare a set of zwitterionic peptoid surface brushes with different spatial separations between charged groups, charge sequence orders, and overall charge densities. It also allowed us straightforward control over the polymer chain length, molecular volume, and surface-grafting density to ensure an unbiased analysis. We characterized antifouling properties through protein adsorption experiments and cell attachment assays involving both mammalian and bacteria cell types. We compared the antifouling performance of zwitterionic versus uncharged polymer brushes. We probed the role of surface hydration, and investigated the length-scale over which a balanced net charge needs to be established to resist fouling. Biomolecules could potentially be attracted to nominally zwitterionic surfaces if individual charged moieties appeared as discrete units on the surface. The results provided insight into the relative roles of surface charge design, surface hydration, and polymer brush structure in controlling non-specific protein–surface and cell–surface interactions.

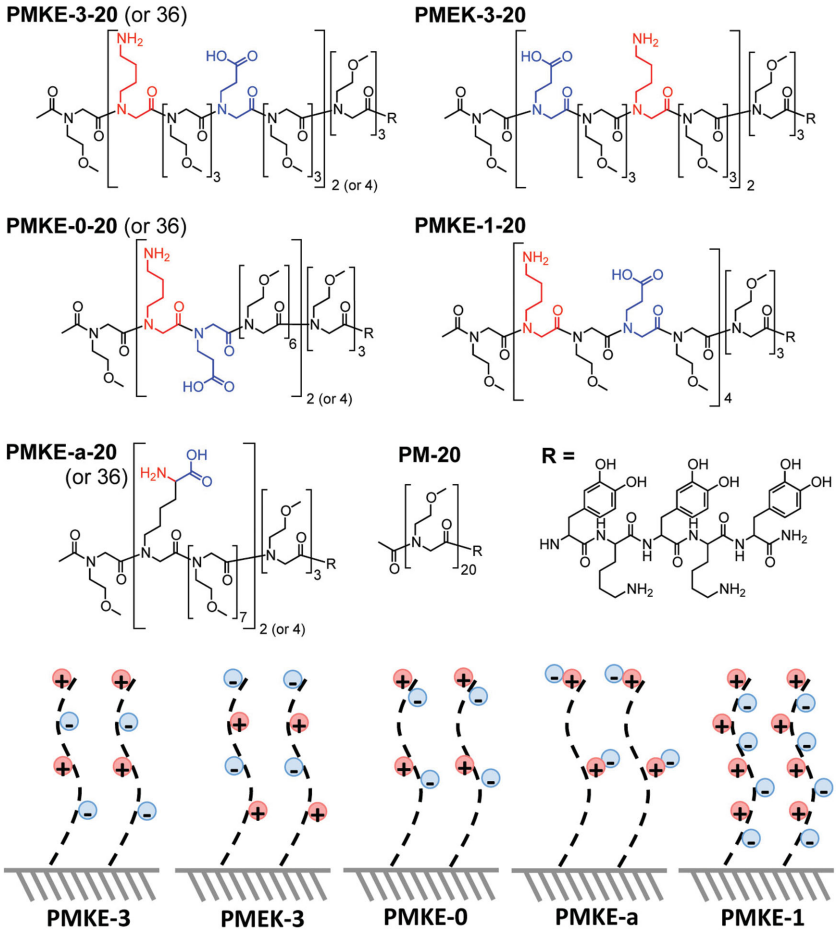

Figure 1. Chemical structures of zwitterionic peptoid model polymers and schematics of the grafted charge arrangement (bottom row). (P: peptoid; M: uncharged spacer residues with methoxyethyl sidechains; K: peptoid analog of lysine (red); E: peptoid analog of glutamic acid (blue).) The number of M residues between the oppositely charged sidechains is indicated by the numeral following the letter designation (0, 1, 3, and a). The last numeral (20 or 36) designates the total number of residues in the peptoid brush segment.

2. Results and Discussion

2.1. Peptoid Model Design and Properties

Peptoids, unlike peptides, have flexible tertiary amide backbones. A series of zwitterionic mixed polyampholytic peptoids with exact residue sequences were designed without structure-inducing sidechains to make them especially suited as antifouling brushes (**Figure 1**). The sequences were prepared by standard submonomer solid phase synthesis and high-pressure liquid chromatography (HPLC) purification (see ESI). Peptoids (P) with equimolar analogs of glutamic acid (E) and lysine (K) were synthesized. These residues were chosen to confer the polyampholytic peptoids a balanced net charge around physiological pH 7.4 (see below). The oppositely charged groups were spaced apart over well-defined distances along the peptoid backbone by inserting uncharged, PEG-inspired residues with methoxyethyl sidechains (M) between them to compose "PMKE" zwitterionic peptoid sequences.

Specific PMKE sequence designs are labeled by the separation between the oppositely charged residues. PMKE-0, PMKE-1, and PMKE-3 refer to separations of, respectively, 0, 1, and 3 uncharged M spacers between the oppositely charged K and E residues. PMKE-a is a special case with both cationic and anion groups placed together on the same sidechain derived from an amino acid (see ESI). The different separations

Table 1. The spatial separations between the oppositely charged groups of the zwitterionic motifs and their ionization behavior.

	PMKE-a	PMKE-0	PMKE-3
Acid-base separation[a)]	0.36 nm (0.35–0.38 nm)	1.1 nm (0.94–1.3 nm)	1.7 nm (1.4–2.0 nm)
pK_a (COOH)[b)]	3.1	4.3	4.3
pK_a (NH_2)[b)]	9.5	10.2	9.8
NH_3^+:COO^-[c)]	992:1000	999:1000	997:1000
%COOH ionized[c)]	100.0%	99.9%	99.9%
pI[b)]	6.3	7.2	7.1

[a)]Average value and, in brackets, range spanning ±2 SD calculated between the oxygen and nitrogen atoms of the ionizable groups from MD simulations; [b)]measured by titration with KOH in 100×10^{-3} M KCl (Figure 2); [c)]calculated at pH 7.4 from the pK_a data obtained from titration measurements (Figure 2 inset).

between the oppositely charged groups were designed to probe the distance over which zwitterionic units need to be structured so as to avoid attractive electrostatic interactions with the discrete charges on protein and cell surfaces.

A sufficient number of uncharged M residues were inserted along the PMKE-a peptoid chains to maintain an identical charge density for all designs except PMKE-1. This had double the number of zwitterionic pairs for investigating the effect of increasing charge density, and expected higher hydration, on antifouling properties.

All designs shared an acetyl-capped uncharged M residue at the N-terminus to preclude chain-end charge effects. Nonetheless, to investigate whether the polarity of the charged residue nearest to the surface of the brush affected antifouling properties, PMEK-3 was synthesized with a reversed sequence order, but with the same charge separation and density, as PMKE-3. PMEK-3 has penultimate negatively charged residues while all other zwitterionic designs have positively charged or zwitterionic residues near their chain ends.

The time-averaged separations between the nearest oppositely charged groups, calculated from atomistic molecular dynamics (MD) simulations, ranged from 0.35 nm (PMKE-a) to 2 nm (PMKE-3; **Table 1** and Figure S1, Supporting Information). Potentiometric titration measurements show that the three archetypical zwitterionic motifs spanning the range of separations between charges (PMKE-3, PMKE-0, and PMKE-a) were all zwitterionic around physiological pH 7.4—fewer than 1 in 100 charge groups were uncompensated by a group of the opposite sign (Table 1 and **Figure 2**).

The surface-grafting peptoids were synthesized on rink amide solid phase resin functionalized with a previously demonstrated bioinspired dihydroxyphenylalanine (DOPA)-containing pentapeptide surface-grafting motif (Figure 1).[17,28–30] The DOPA motif, prepared by standard Fmoc solid phase peptide synthesis and cleaved together with the peptoid segment, enabled the grafting of the peptoids onto a prototypical biomedical device substrate (TiO_2) with facile control over the surface chain density (see Section 2.2.1).[17,30]

The archetypical PMKE-3, PMKE-0, and PMKE-a peptoids were synthesized with 20 and 36 residues (Figure 1). The chain lengths are indicated at the end of the sequence designation (e.g., PMKE-3–20 and PMKE-3–36). This probes the chain length dependence of the antifouling effect.[16,17]

The selection of M residues as the uncharged spacer offered two important properties. First, homopolymer peptoid brushes composed of this residue (PM-20) were previously shown to exhibit excellent resistance against protein adsorption and long-term cell attachment.[17,28] Accordingly PM-20 was used as the uncharged control in this study to explicitly probe whether the zwitterionic character of the PMKE designs conferred any additional benefit in terms of antifouling properties. Second, the use of uncharged M spacer residues, rather than other antifouling peptoid designs (e.g., polysarcosine),[17] led to very similar molecular volumes across all peptoid sequences. For example, MD models show there is only a 1.6% difference in molecular volumes between the peptoid segments of PM-20 and PMKE-3–20 (2.78 nm^3 vs 2.82 nm^3). The ability of a surface-grafted polymer brush to resist protein adsorption depends also on the molecular volume of the monomers, which help determine the volume exclusion of proteins from the surface.[14–16] This parameter is difficult to manipulate with other polymer designs. In this study, the small differences in molecular volumes of the different designs are unlikely to contribute significantly to possible differences in antifouling properties, which can instead be more directly attributed to differences in the chemical natures of the peptoid sequences.

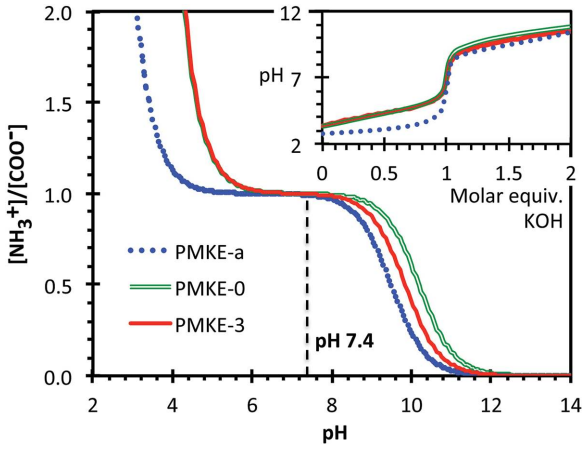

Figure 2. The ratio of protonated amines to deprotonated carboxylic acids of model peptoid sequences as a function of pH. The curves are calculated from the pK_a (Table 1) measured from potentiometric titration measurements of peptoid solutions (inset). Model PMKE zwitterionic motifs without the DOPA adhesive pentapeptide (Figure S2, Supporting Information) were synthesized for these measurements.

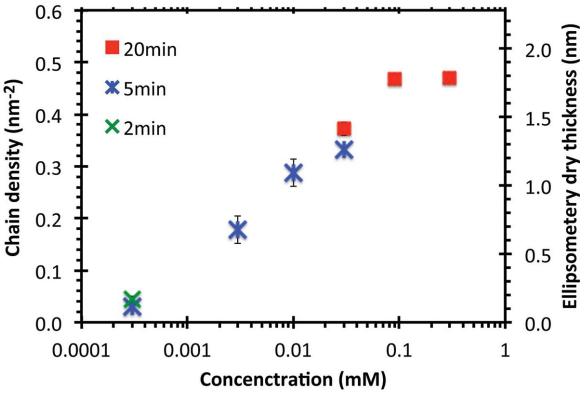

Figure 3. The grafted surface chain density of PMKE-a-20 at different coating durations and solution concentrations. The left axis shows the corresponding dry film thickness as measured by ellipsometry. The error bars indicate ±1 SD.

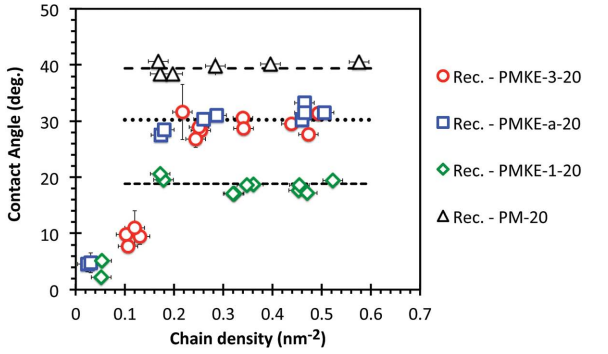

Figure 4. Receding water contact angles on the peptoid brushes (20-mers; ˆ – PMKE-3–20, □ – PMKE-a-20, ◇ – PMKE-1–20, △ – PM-20). The dashed lines indicate the values (averages) of the respective receding angle plateaus. The horizontal error bars indicate 0.02 nm^{-2}, and the vertical error bars indicate ±1 SD.

2.2. Peptoid Polymer Brush Surface Characterization

2.2.1. Peptoid Surface Grafting

The grafted chain densities of the various PMKE peptoids were controlled by modifying the coating duration and solution concentration. Details of the approach have been previously reported.[17,30] **Figure 3** shows, using PMKE-a-20 as example, the ability to control the grafted surface chain density over an order of magnitude up to ~0.5 nm^{-2}. Results for the other peptoids are shown in Figure S3, Supporting Information. A dry thickness of 2 nm corresponds to a swollen ≈6-nm-thick brush layer in aqueous solution, as measured by liquid AFM.[30] In comparison, the contour length of the 20-mer peptoids including the DOPA pentapeptide anchor is 8.5 nm based on the 0.34 nm monomer length of single amino acid residues. A chain density of ≈1 nm^{-2} is the maximum possible for a brush monolayer based on the dimensions of the DOPA pentapeptide anchor.[17,30]

As expected, the grafted surface chain density increased with longer coating durations and higher peptoid concentration. The grafting density obtained after a certain coating duration followed a log–linear relationship with the concentration, up to an asymptotic value. Therefore the chain density could be more predictably controlled by changes in concentration than in coating duration, which is clearly shown for PMKE-a-20 in Figure 3.

2.2.2. Hydration Characterization by Water Contact Angle Measurements

Figure 4 compares the receding water contact angle data for PMKE-3–20, PMKE-a-20, and PMKE-1–20, which are representative of the various peptoid designs with different charge arrangements and densities, with the uncharged PM-20 control. The receding angle characterizes how well a previously submerged peptoid surface binds to water as it is re-exposed to air. Water contact angles were measured over the entire range of grafted peptoid chain densities used for the characterization of antifouling properties (Sections 2.3 and 2.4). Lower angles indicate a more favorable interaction with water.

The receding angles of the 20-mer zwitterionic designs increased asymptotically from near complete wetting to specific plateau values ($\theta_{plateau}$) at chain densities > 0.2 chain nm^{-2}. PMKE-3–20 and PMKE-a-20, which have the same sequence charge density, exhibited a $\theta_{plateau} \approx 30°$. Indeed, other zwitterionic designs with the same charge density also exhibited the same $\theta_{plateau} \approx 30°$ (Figure S4A, Supporting Information). In comparison, PMKE-1–20, which has double the number of charge groups as the other peptoid brushes exhibited a lower $\theta_{plateau} \approx 19°$, while the uncharged PM-20 exhibited a higher $\theta_{plateau} \approx 39°$ (Figure 4). In contrast, both bare TiO_2 and a surface covered solely by the DOPA surface anchor pentapeptide without peptoid segments, could be completely wetted by water in receding angle measurements (contact angles < 5°).[17]

The existence of $\theta_{plateau}$ showed that the peptoids were able to effectively cover the surface and exclude the completely wetting interactions of the TiO_2 substrate and DOPA anchor at sufficiently high chain densities. Moreover, the relative magnitudes of $\theta_{plateau}$ (PMKE-1–20 < PMKE-3–20 and other peptoids with the same charge density < PM-20) showed that surface hydration increased with higher densities of charged groups along a peptoid sequence. This is consistent with the fact that charged groups generally exhibit better hydration, via both hydrogen bonding and ionic interactions with water, than their uncharged counterparts.[19] Analytical HPLC measurements of the peptoids in solution showed a similar trend in relative water solubility (Figure S5, Supporting Information).

It was also observed that the values of $\theta_{plateau}$ did not depend on the chain length. Figure 4 and Figure S4 (Supporting Information) show that the 20- and 36-mers of the same charge separation designs exhibited identical $\theta_{plateau}$, and Figure S4 (Supporting Information) also shows an identical $\theta_{plateau}$ for both PM-20 and PM-50. A chain-length independent $\theta_{plateau}$ is consistent with the grafting of the peptoid chains in the intended orientation extending away from the substrate, and concealing the DOPA anchors (Figure 1). In contrast, if the peptoids were deposited with mixed orientations and some of the DOPA pentapeptide anchors were exposed to water, the receding angles would depend on the chain length—the DOPA

anchors constitute a larger fraction of the molecules for shorter peptoid chains, and would have exerted a larger influence on the wetting behavior.

The advancing angle data are also shown in Figure S4, Supporting Information. These results are less relevant to the present study as they reflect the initial wetting behavior of dried peptoid surfaces, and do not impact antifouling properties in aqueous environments. Briefly, all zwitterionic designs show essentially identical behavior, with advancing angles increasing from complete wetting at low grafted chain densities to a maximum of approximately 50° at intermediate densities before decreasing gradually to <40° with further increases in chain densities. The closely matching behavior could reflect the fact that all PMKE share the same chemical building blocks and acetyl-capped terminal M residues. In contrast to the initially increasing and then decreasing behavior of the PMKE surfaces, the advancing angle on the uncharged control remained constant at ~40° even at high chain densities. This suggests that the advancing angle behavior of the PMKE peptoids originated from variations in the initial ionization or charge arrangement of the dried peptoids with increasing grafted chain density (e.g., pairing of opposite charges). However, this is not interpreted further as there is no simple relationship between contact angles and the microscopic details of chain conformations.[31]

2.2.3. Surface Charge Behavior Probed by Avidin Adsorption

Avidin (67 kDa; ≈6 nm diameter) was chosen as a "nanoprobe" to investigate the surface charge behavior of the grafted zwitterionic peptoids. It is a unique protein that maintains, between pH 4 and 8, a relatively constant folded structure, size, and positive charge (isoelectric point: $pI_{avidin} = 9$).[32] This physicochemical stability means that variations in the protein's adsorption would depend predominately on charge effects of the surface over this pH range. A relatively low ionic strength (10×10^{-3} M buffer), and an intermediate chain density (see Section 2.3), was used to emphasize the electrostatic interactions on antifouling brushes that are expected to exhibit low protein adsorption.

Figure 5A illustrates the surface charge characterization with avidin adsorption on the TiO_2 substrate. Below $pI_{TiO2} = 5–6$,[33] both avidin and TiO_2 were positively charged and electrostatically repelled each other, and a relatively low amount of adsorption, possible controlled by van der Waals interactions, was observed (90 ng cm^{-2} at pH 4). Above pH 7.4, the repulsion between neighboring proteins decreased as the pH approached pI_{avidin}, and adsorption was high (312 ng cm^{-2} at pH 8.2). However, over pH 5–7.4, a relatively constant intermediate amount of adsorption was observed (≈240 ng cm^{-2}, corresponding to a monolayer,[34] indicating relatively stable charge behavior of both avidin and TiO_2. Therefore, the analysis below focuses on this pH range.

Figure 5B and C shows that adsorption on the antifouling peptoid brush surfaces was much lower than on TiO_2 but nonetheless depended on the pH and the charge sequence design. The peptoids PMKE-3–20, PMKE-0–20, and PMKE-a-20, which exhibit the same sequence charge densities and span the range of spatial separations between opposite charges studied, were compared with the uncharged PM-20 control and with

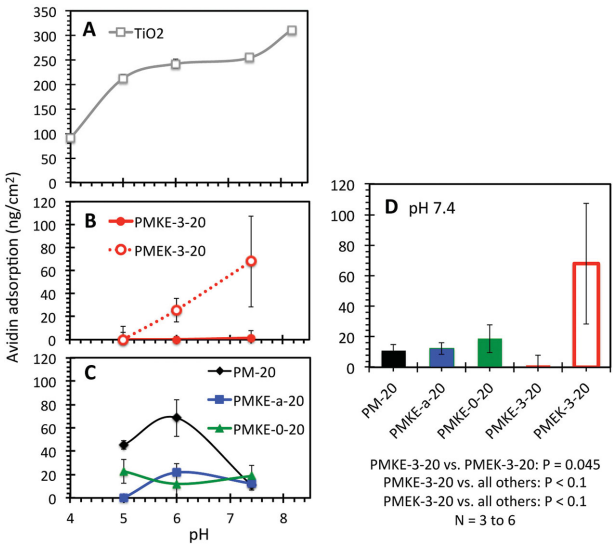

Figure 5. A–C) Avidin adsorption on the archetypical peptoid brushes and TiO_2 control. Samples were exposed to avidin solution (1.5×10^{-6} M in 10×10^{-3} M buffer) for 30 min at 37 °C. The amount of irreversibly adsorbed avidin was measured by ellipsometry after sample rinsing. The surface chain density was 0.31 ± 0.03 nm^{-2} for all brushes. The data points are connected by smoothed lines. D) Summary of the adsorption results at pH 7.4. *P* values of unpaired *t* tests between the designs are listed below the figure. Error bars for all panels indicate ±1 SD. $N \geq 3$.

PMEK-3–20, which has the reversed charge sequence order as PMKE-3–20.

Figure 5B contrasts the adsorption on PMKE-3–20 and PMEK-3–20 brushes, which share the same widest charge separation among the peptoid designs but have, respectively, basic and acidic residues near their chain ends (Figure 1). This switch resulted in increasing avidin adsorption from pH 5 to 7.4 on PMEK-3–20, but negligible adsorption on PMKE-3–20. Evidently, the electrostatic interaction was strongly associated with the polarity of the terminal charged residues on the PMKE/PMEK-3–20 brushes—a more negatively charged surface can more strongly attract the positively charged avidin. The measured pK_a's (Table 1) indicate that the fraction of ionized, negatively charged acidic sidechains would rise from 82% to 100% over pH 5–7.4, while ~100% of the basic sidechains would remain positively charged throughout. Therefore both PMKE and PMEK-3–20 should have an overall zwitterionic character as the pH increased to 7.4. To reconcile this ionization behavior with the observed adsorption, it would appear that the charge groups along the PMKE and PMEK-3–20 chains were placed far enough apart that avidin experienced much better access to the terminal charge groups that were presented, on average, on the brush surface. The ionic strength was also apparently not high enough ($\lambda_{Debye} \approx 2$ nm) to screen this surface charge effect.

Figure 5C shows that small amounts of avidin were adsorbed on PMKE-a-20 and PMKE-0–20 (≲30 ng cm^{-2}) throughout the pH range tested. No obvious trend was observed. PMKE-0–20 has a positively charged terminal residue like PMKE-3–20, while PMKE-a-20 has zwitterionic sidechains. Both PMKE-a-20 and PMKE-0–20, however, have the pairs of oppositely charged groups more closely spaced together than in PMKE/PMEK-3–20 (0.36 and 1.1 nm vs 1.7 nm; Table 1). Therefore,

the results indicate that the opposite charges were close enough to mutually screen each other, thus constituting zwitterionic, net neutral PMKE-0–20 and PMKE-a-20 brushes to repel protein adsorption. (At pH 5, the PMKE-0–20 surface may have an ≈28% excess of positive charges, but this would also help to repel the positively charged avidin).

Although surface induced changes to the degree of ionization is possible, our results do not indicate a significant effect. For example, a suppressed ionization of base groups on the surface could be consistent with the lower adsorption on PMKE-3–20 than on PMEK-3–20, but would also have led to increasing excess negative charge and adsorption with pH on PMKE-0–20 and PMKE-a-20, which was not observed. The different surface charging scenarios that may or may not be consistent with the present results are illustrated in Figure S7, Supporting Information.

Figure 5C also shows that adsorption on the uncharged PM-20 went through a maximum (~80 ng cm^{-2}) between pH 5 and 6 that coincided with pI_{TiO2} (Figure 5C). While this might have been coincidental, proteins very close to the surface could have sampled a partial substrate charge effect through the brush monolayer.[35] In contrast, the PMKE peptoids appeared to be able to screen most of this substrate effect. A higher ionic strength was also able to screen this charge effect on PM-20 (Figure S6, Supporting Information).

Figure 5D summarizes the avidin adsorption results at physiological pH 7.4. PMKE-a-20 and PMKE-0–20, with short spatial separations between opposite charges, exhibited a level of protein adsorption that was similar to the uncharged PM-20 brush and behaved effectively as zwitterionic brushes. On the other hand, the opposing results on PMKE/PMEK-3–20 indicate that the charge groups were sufficiently separated that the groups near the brush surface became more accessible to incoming proteins. The surface charge can then, *if* the solution ionic strength were insufficient to screen the charges, be dominated by the polarity of the terminal charges on the polymer brush.

2.3. Resistance against Protein Adsorption at Physiological pH and Ionic Strength

The short-term resistance against protein adsorption is commonly measured to evaluate the performance of an antifouling surface, since protein adsorption occurs rapidly and mediates subsequent cell–surface interactions.[8,36] A first set of experiments used fibrinogen (Fg) as a model protein, which is a large biomacromolecule presenting multiple charged amino acid residues on its surface (340 kDa; ≈6 × 6 × 48 nm^3)[37] that could interact with and challenge the zwitterionic brushes. Fg is also a major component of blood proteins relevant to important physiological responses against biomaterials such as surface-induced thrombosis and inflammation.[38] A second set of experiments investigated adsorption from 10% serum. Blood serum contains over 1000 proteins of different sizes and net electrostatic charges[39] that could challenge the peptoid brushes in different ways. The 10% serum solution was also used for mammalian cell culture experiments (see next section), and characterization of its adsorption helps to interpret the resistance of the peptoid brushes against nonspecific cell attachment. In contrast to the avidin surface charge experiments, all Fg and serum adsorption experiments were performed at a physiological pH and ionic strength.

Figure 6 shows the amount of proteins adsorbed as a function of the peptoid chain density at 20-mer chain length. Results for the 36-mers are shown in Figure S8, Supporting Information. Theoretical analysis indicates that the equilibrium amount of protein adsorption on polymer brushes depends not only on the chemical nature of the polymer brush and the protein, but also critically on the chain density and chain length—adsorption generally decreases with increasing chain density and chain length.[16,17] Accordingly, protein adsorption decreased monotonically from levels similar to that on the bare TiO_2 control at <0.1 chain nm^{-2}, to being essentially inhibited at sufficiently high densities. The generally higher amounts of adsorbed Fg over serum reflect the higher molecular weight (M_w) of Fg compared to the average in serum, which has a large component of serum albumin (M_w = 66 kDa).[39]

Slightly lower levels of Fg adsorption on the zwitterionic 20-mer brushes than on the uncharged PM-20 were observed

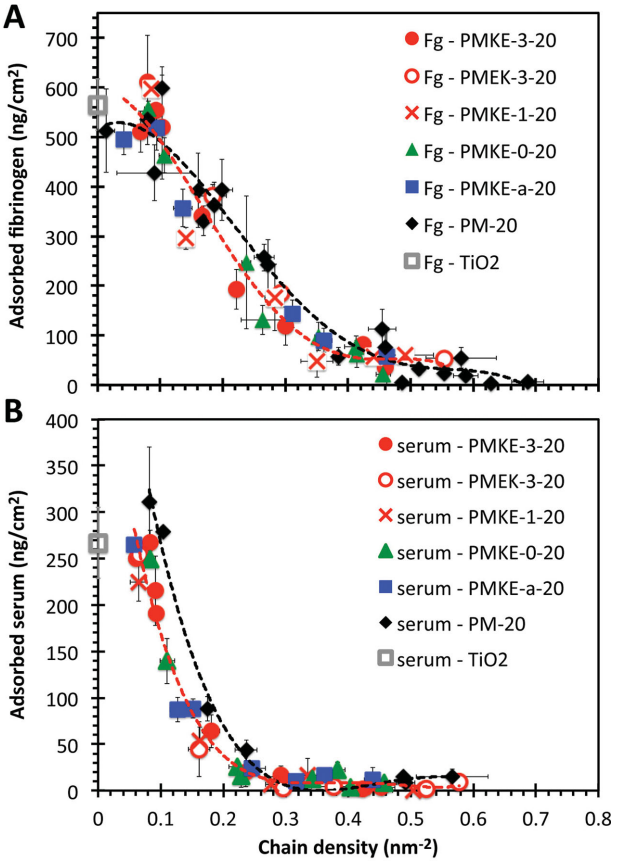

Figure 6. Irreversible protein adsorption on the zwitterionic PMKE peptoid 20-mer brushes as a function of grafted chain density. A) shows the amount of adsorption from 4 × 10^{-6} M fibrinogen (Fg) in 10 × 10^{-3} M hepes and 150 mM NaCl. B) shows adsorption from cell culture media with 10% bovine calf serum (serum). Both solutions were at pH 7.4. The samples were immersed for 20 min at 37 °C, rinsed and then measured by ellipsometry. $N \geq 3$. The error bars indicate ±1 SD. The dashed lines are fourth degree polynomial fits: black dashes represent the PM-20 data; red dashes represent simultaneous fits to all PMKE/PMEK data shown.

at intermediate chain densities in these short-term experiments (0.2–0.3 chain nm^{-2}; Figure 6A). When challenged with serum proteins, slightly lower adsorption was observed on the zwitterionic brushes than on PM-20 at <0.25 chain nm^{-2} (Figure 6B). However, the different spatial separations and sequence arrangements between the oppositely charged groups of the various PMKE/PMEK peptoids, in contrast to the situation with avidin adsorption at low ionic strength, did not appear to influence protein adsorption.

At higher chain densities, all peptoid brushes could resist protein adsorption to similar degrees. A small amount of Fg adsorption (20–100 ng cm^{-2}) was observed for all peptoid designs at 0.4–0.6 chain nm^{-2} before being prevented at a critical density ≈0.6 chain nm^{-2} (adsorption below the measurement uncertainty of ≈10 ng cm^{-2}). Serum adsorption on all peptoid designs decreased from ≈20 ng cm^{-2} to ≈10 ng cm^{-2} as the chain density increased from 0.25 to 0.6 chain nm^{-2} (Figure S9, Supporting Information), consistent with a "critical"[17] density of ≈0.6 chain nm^{-2}.

The adsorption on the 36-mers was analogous. No discernible difference was observed between PMKE-3–36, PMKE-0–36, and PMKE-a-36. In line with theoretical expectations, the trends were shifted toward lower chain densities (Figure S8, Supporting Information) because a longer chain has more steric bulk than a shorter chain at the same chain density.[17]

The zwitterionic peptoids share the same polar peptoid backbone, most of the same residues, and occupy similar molecular volumes as the uncharged control (see Section 2). Therefore, the moderate decrease in adsorption observed on the zwitterionic brushes compared with the uncharged control is directly correlated with the zwitterionic nature of the brushes. At the same time, the similarity in adsorption between the different zwitterionic designs indicates that the criteria for the arrangement of opposite charges for imparting an effective zwitterionic character to the polymer brushes are relatively flexible. At physiological ionic strength, individual charges are screened even up to very short distances (λ_{Debye} = 0.7 nm). Therefore, separating the oppositely charged groups even up to three spacer residues in PMKE-3 (1.7 nm on average; see Table 1) did not influence protein adsorption.

Contact angle measurements show that the uncharged PM-20 has a much higher $\theta_{plateau}$ = 39° than those for the zwitterionic peptoids (Figure 4), indicating a lower hydration of the uncharged brush. A binary comparison between PM-20 and any one of the archetypical peptoids (i.e., PMKE-3, PMKE-0, and PMKE-a; $\theta_{plateau}$ ≈ 30°) might suggest that higher hydration could lead to the slightly reduced protein adsorption at intermediate chain densities. However PMKE-1–20, which has twice the number of charged groups as PMKE-3–20 and even higher hydration, resisted protein adsorption at a level similar to the rest of the zwitterionic brushes. This indicated first that the performance of the PMKE peptoids was not limited by the number of charged groups in the designs. It also suggested that increased hydration alone cannot explain the slightly lower short-term protein adsorption on the zwitterionic brushes. Instead, a balanced electrostatic interaction, or the mode of hydration (e.g., ionic vs hydrogen bonding), could be important.

Comparisons in the literature concerning the difference in resistance against protein adsorption between zwitterionic and uncharged polymer brushes are frequently performed with limited control in the grafted chain densities, chain lengths, or molecular volumes.[18,20,23,25] Figure 6 shows that, at a constant chain length, only a small difference between the zwitterionic brushes and the uncharged PM-20 control could be observed at intermediate chain densities, which could easily have been obscured if brushes grafted at different chain densities were compared. This, however, also implies that the practical significance of this difference would be small.

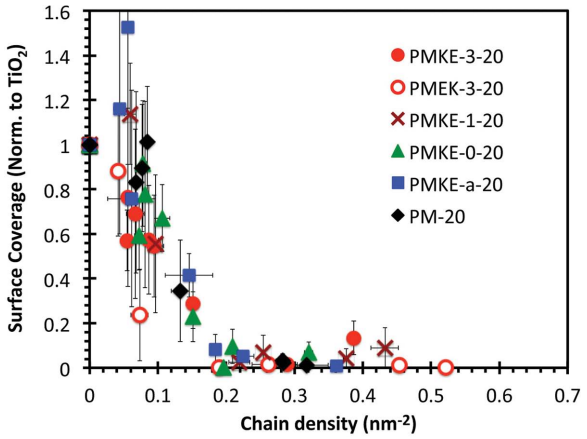

Figure 7. Mammalian cell attachment on the zwitterionic PMKE peptoid brushes as a function of grafted chain density. The surface coverages of live 3T3 swiss albino mouse fibroblasts attached on the peptoid surfaces (4-d culture) were normalized to the TiO_2 controls corresponding to each series. The initial seeding density was 2500 cells cm^{-2}. The average on TiO_2 across all series was 33 ± 18%. $N \geq 3$. The error bars indicate ±1 SD.

2.4. Resistance against Mammalian and Bacterial Cell Attachment

Figure 7 shows the surface coverage of 3T3 mouse fibroblasts attached on the peptoid brushes as a function of the grafted chain density, normalized to the coverage on bare TiO_2 controls. **Figure 8** shows the coverages of both gram-positive (*Staphylococcus aureus* and *Staphylococcus epidermidis*) and gram-negative (*Escherichia coli* and *Pseudomonas aureginosa*) bacteria strains attached on the peptoid surfaces. Fibroblasts are responsible for collagen synthesis during wound healing, but excessive fibroblast activation and subsequent fibrosis around a biomedical device may be deleterious to device function.[36] The bacteria strains were selected for their relevance to medical device related infection.[40] According to accepted protocol,[30,41] the bacterial assay was performed in saline solution without growth media to specifically provide a fair test of the resistance against the initial attachment of bacteria.

The general trend of fibroblast attachment with varying peptoid chain density followed that of protein adsorption. As peptoid densities increased fibroblast attachment decreased monotonically, from levels similar to that on the TiO_2 control, to being essentially prevented above a critical grafting density (Figure 7). However, the modest difference between the zwitterionic and uncharged PM-20 brushes was no longer observed. Lower attachment on PMEK-3–20 compared to the other peptoid

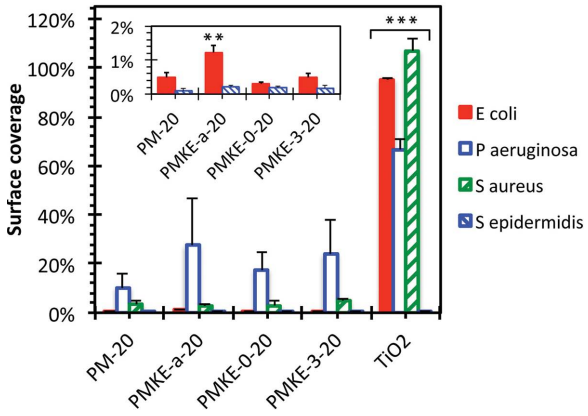

Figure 8. The ability of the peptoid brushes to resist attachment of bacteria (as surface coverage of both live and dead cells attached after 24 h in 150×10^{-3} M NaCl and after gentle rinsing). The inset shows the low coverages recorded for *E. coli* and *S. epidermidis* attachment. The initial seeded density for all strains were ~1×10^8 CFU mL^{-1}. All brushes were grafted at 0.3 ± 0.015 chain nm^{-2}. (***) indicates $P < 0.001$; (**) indicates $P < 0.01$. $N \geq 3$. The error bars indicate ±1 SD.

brushes was observed at 0.075 chain nm^{-2} but the difference was not statistically significant. Fibroblast attachment was essentially inhibited at a critical chain density of ≈0.2 chain nm^{-2}. The analogous behavior was replicated on the longer 36-mers, except that the trends were scaled, as with protein adsorption on the 36 versus the 20-mers, to lower chain densities. A critical density of ≈0.15 chain nm^{-2} was observed on the 36-mers (Figure S10, Supporting Information).

The lack of a difference in fibroblast attachment between the zwitterionic and uncharged peptoid brushes could indicate that the slight advantage in preventing protein adsorption enjoyed by the zwitterionic brushes was a short-term kinetic effect.[16] Fibroblast attachment was recorded after 4 d, to allow the cells time to attach, sample the surface and proliferate (given appropriate surface conditions). Attachment results after 1 d showed a broadly similar trend as the 4-d results, but the uncertainty in the data was high (Figure S11, Supporting Information). Although previous measurements on PM-20 did not reveal a difference in protein adsorption up to 18 h,[17] it is possible that the amount of proteins adsorbed on the zwitterionic brushes, including the adsorption of extracellular matrix proteins secreted by the cells themselves, could have increased over time to the same level as on the uncharged control. Accurate monitoring of protein adsorption beyond 24 h is difficult.[42] In fact, long-term monitoring of cell attachment has been used as a proxy for long-term protein adsorption.[28,30,43]

The present results represent the first detailed characterization of cell attachment on zwitterionic polymer brushes over a wide range of grafting density. It showed that fibroblast attachment on the zwitterionic brushes generally depended on the amount of serum adsorption, just as on the uncharged PM-20 brush, as well as on PEG polymer brushes.[44] The critical chain density for preventing cell attachment (0.2 chain nm^{-2}) was slightly lower than that for preventing serum adsorption. At 0.2 chain nm^{-2}, the amount of serum adsorption was 30–50 ng cm^{-2}. This is consistent with previous findings showing that cell attachment required a threshold level of cell adhesion ligands present on serum proteins.[44,45] Possibly contrary to expectations, the resistance against fibroblast attachment did not appear to depend on the chemical nature of the antifouling brush.

To more sensitively characterize cell attachment behavior on the different sequence designs, the archetypical PMKE-3–20, PMKE-0–20, and PMKE-a-20 peptoid brushes were challenged with high concentration suspensions of four bacteria strains (10^8 CFU mL^{-1}). The cell membranes of different bacteria strains can be highly varied, and many bacteria species have a higher ability than mammalian cells to attach to surfaces.[46] Consequently, many antifouling polymer brushes that can resist mammalian cell attachment are unable to resist fouling by at least some bacteria strains.[47] To further help discern possible differences between the sequence designs, the experiments were performed at an intermediate chain density (0.3 ± 0.015 chain nm^{-2}) that was only expected to partially resist bacteria attachment.

Figure 8 shows that all the peptoid surfaces, zwitterionic or uncharged, were able to significantly reduce bacteria attachment relative to the bare TiO_2 control ($P < 0.001$). The amount of attached bacteria was observed in the following order: *P. aureginosa* > *S. aureus* > *E. coli* > *S. epidermidis*. Bacteria attachment did not appear to depend on whether the bacteria strain was gram-positive (*S. aureus and S. epidermidis*) or negative (*P. aureginosa* and *E. coli*).

However, small but statistically significant differences were observed between PMKE-a-20 and the other brush surfaces: this brush design was slightly less resistant against *E. coli* attachment than the other peptoid brushes (99% vs ≥99.6% reduction; $P < 0.01$), and only ≈5% of the small number (≈0.2% coverage) of the *S. epidermidis* attached on PMKE-a-20 did not retain intact membranes (i.e., they had died; Figure S12, Supporting Information). On all other brushes, a much higher 40%–50% of the attached bacteria had died by the end of the 24-h assay.

Specific molecular interactions could have contributed to the subtle differences observed in the case of PMKE-a-20. This design presented zwitterionic sidechains that were, among the peptoid sequences, most similar in chemical structure to the antifouling polybetaine designs that have been suggested to preserve the secondary structure of adsorbed proteins.[48] Even though this characteristic did not produce differences in the overall resistance against protein adsorption and fibroblast attachment, it might have influenced antifouling properties in specific cases, such as in allowing the small number of attached *S. epidermidis* to stay alive, and the slightly increased attachment of *E. Coli*.

3. Conclusions

We designed and synthesized a set of sequence-specific, zwitterionic peptoid polymers, and investigated the molecular features contributing to the antifouling properties of surface-grafted polymer brushes. The peptoid system allowed us precise control over a range of molecular features that impact on antifouling properties, but may be difficult to simultaneously specify with other polymer models. These included the polymer

charge density and hydration, the polymer chain length and grafted density, the molecular volume of the set of model polymers, the intrinsic antifouling capability of the polymer system, and the spatial separation between charge groups.

Our results show that, at physiological ionic strength, the antifouling properties of mixed zwitterionic brushes could be maintained even when the oppositely charged groups were separated up to the largest distance tested (1.7 nm), which is a significant fraction of a typical protein's dimensions. This tolerance in the range of spatial separation justifies the preparation of zwitterionic antifouling polymer brushes by random copolymerization of a balanced ratio of monomers bearing opposite charges, which can be synthetically more convenient than polymer brushes bearing zwitterionic betaine sidechains. However, at a sufficiently low ionic strength, the polarity of the charged residue near the termini of the polymer chains (i.e., those dwelling near the top of the brush on average) could determine the electrostatic interaction of proteins with the surface.

Although (mixed) zwitterionic brushes could offer advantages such as further functionalization through some of the acid or basic groups,[18] and phosphorylcholine-based brushes have shown an advantage in suppressing the inflammatory response against foreign-implanted material,[49] our modular peptoid model showed that the addition of zwitterionic elements to a polymer brush already possessing antifouling properties conferred at most a modest benefit to resisting short-term protein adsorption, and did not increase the resistance against mammalian and bacterial cell attachment. Through the unprecedented simultaneous control of a comprehensive range of chemical, physical, and physico-chemical molecular features, we demonstrate in a single well-defined system, the dominating effects of chain length and density on the performance of antifouling polymer brushes. These results further suggest that it might be worthwhile to consider aspects of molecular design that may only be implicitly linked to chemical interactions, such as polymer surface arrangement and conformational flexibility, to improving antifouling properties. We envision that peptoids may also be fruitfully applied to investigating the molecular features of other biointerfacial systems.

Supporting Information

The Experimental Methods, the materials used and the Supporting Information are available from the Wiley Online Library or from the author.

Acknowledgements

This research was supported by Grant No. EB005772 from the National Institute of Biomedical Imaging and Bioengineering (NIBIB) at the National Institutes of Health (NIH). K.H.A.L. acknowledges support by fellowship number HL104966 from the National Heart, Blood and Lung Institute (NHBLI) at the NIH. T.S.S. was funded by a National Science Foundation Graduate Fellowship (NSF GRFP 2011124091) and The Ryan Fellowship. K.H.A.L. and A.M.L.S. acknowledge support by the University of Strathclyde Academic Investment Scheme. P.B. acknowledges postdoctoral fellowship support from the Swiss National Science Foundation (Project No. 151860). The authors gratefully acknowledge Ran Zhang and especially Jin Tao for technical support. MALDI-MS was performed at the Integrated Molecular Structure Education and Research Center (IMSERC) at Northwestern University (NU) with generous support by NU/State of Illinois. Boc-Lys-OtBu was synthesized by ChemCore at the Center for Molecular Innovation and Drug Discovery (CMIDD) which is generously supported by the Chicago Biomedical Consortium with support from The Searle Funds at The Chicago Community Trust. Peptoid synthesis at the Molecular Foundry (User Proposal No.1523) was supported by the Office of Science, Office of Basic Energy Sciences, of the US Department of Energy under Contract No. DE-AC02–05CH11231. We are grateful for the assistance given by Drs. R. N. Zuckermann, M. Connolly, G. Olivier and A. Rosales at the Molecular Foundry.

Received: May 5, 2014
Revised: October 12, 2014
Published online: November 26, 2014

[1] J. Sun, R. N. Zuckermann, *ACS Nano* **2013**, *7*, 4715.
[2] A. S. Culf, R. J. Ouellette, *Molecules* **2010**, *15*, 5282.
[3] J. A. W. Kruijtzer, L. J. F. Hofmeyer, W. Heerma, C. Versluis, R. M. J. Liskamp, *Eur. J. Chem.* **1998**, *4*, 1570.
[4] a) S. A. Fowler, H. E. Blackwell, *Org. Biomol. Chem.* **2009**, *7*, 1508; b) M. T. Dohm, R. Kapoor, A. E. Barron, *Curr. Pharm. Des.* **2011**, *17*, 2732.
[5] A. M. Rosales, R. A. Segalman, R. N. Zuckermann, *Soft Matter.* **2013**, *9*, 8400.
[6] K. H. A. Lau, *Biomater. Sci.* **2014**, *2*, 627.
[7] S. Krishnan, C. J. Weinman, C. K. Ober, *J. Mater. Chem.* **2008**, *18*, 3405.
[8] C. Blaszykowski, S. Sheikh, M. Thompson, *Chem. Soc. Rev.* **2012**, *41*, 5599.
[9] E. Ostuni, R. G. Chapman, M. N. Liang, G. Meluleni, G. Pier, D. E. Ingber, G. M. Whitesides, *Langmuir* **2001**, *17*, 6336.
[10] A. A. Shemetov, I. Nabiev, A. Sukhanova, *ACS Nano.* **2012**, *6*, 4585.
[11] P. Lin, C. W. Lin, R. Mansour, F. Gu, *Biosensors Bioelectron.* **2013**, *47*, 451.
[12] T. Merian, J. M. Goddard, J. Agric, *Food Chem.* **2012**, *60*, 2943.
[13] S. Herrwerth, W. Eck, S. Reinhardt, M. Grunze, *J. Am. Chem. Soc.* **2003**, *125*, 9359.
[14] I. Szleifer, *Biophys. J.* **1997**, *72*, 595.
[15] J. Satulovsky, M. A. Carignano, I. Szleifer, *Proc. Natl. Acad. Sci. U S A* **2000**, *97*, 9037.
[16] F. Fang, J. Satulovsky, I. Szleifer, *Biophys. J.* **2005**, *89*, 1516.
[17] K. H. A. Lau, C. Ren, S. H. Park, I. Szleifer, P. B. Messersmith, *Langmuir* **2012**, *28*, 2288.
[18] S. Y. Jiang, Z. Q. Cao, *Adv. Mater.* **2010**, *22*, 920.
[19] S. F. Chen, L. Y. Li, C. Zhao, J. Zheng, *Polymer* **2010**, *51*, 5283.
[20] S. F. Chen, S. Y. Jiang, *Adv. Mater.* **2008**, *20*, 335.
[21] R. E. Holmlin, X. X. Chen, R. G. Chapman, S. Takayama, G. M. Whitesides, *Langmuir* **2001**, *17*, 2841.
[22] C. H. Shen, J. C. Lin, *Langmuir* **2011**, *27*, 7091.
[23] S. Tada, C. Inaba, K. Mizukami, S. Fujishita, M. Gemmei-Ide, H. Kitano, A. Mochizuki, M. Tanaka, T. Matsunaga, *Macromol. Biosci.* **2009**, *9*, 63.
[24] E. Beurer, N. V. Venkataraman, M. Sommer, N. D. Spencer, *Langmuir* **2012**, *28*, 3159.
[25] W. Feng, S. P. Zhu, K. Ishihara, J. L. Brash, *Biointerphases* **2006**, *1*, 50.
[26] K. Tamada, M. Hara, H. Sasabe, W. Knoll, *Langmuir* **1997**, *13*, 1558.
[27] a) N. D. Brault, H. S. Sundaram, Y. T. Li, C. J. Huang, Q. M. Yu, S. Y. Jiang, *Biomacromolecules* **2012**, *13*, 589; b) Y. Chang, S. H. Shu,

Y. J. Shih, C. W. Chu, R. C. Ruaan, W. Y. Chen, *Langmuir* **2010**, *26*, 3522.
[28] A. R. Statz, R. J. Meagher, A. E. Barron, P. B. Messersmith, *J. Am. Chem. Soc.* **2005**, *127*, 7972.
[29] A. R. Statz, J. P. Park, N. P. Chongsiriwatana, A. E. Barron, P. B. Messersmith, *Biofouling* **2008**, *24*, 439.
[30] K. H. A. Lau, C. Ren, T. S. Sileika, S. H. Park, I. Szleifer, P. B. Messersmith, *Langmuir* **2012**, *28*, 16099.
[31] S. H. Park, M. A. Carignano, R. J. Nap, I. Szleifer, *Soft Matter.* **2010**, *6*, 1644.
[32] M. Firnkes, D. Pedone, J. Knezevic, M. Döblinger, U. Rant, *Nano Lett.* **2010**, *10*, 2162.
[33] J. W. Bullard, M. J. Cima, *Langmuir* **2006**, *22*, 10264.
[34] D. Clerc, W. Lukosz, *Biosensors Bioelectron.* **1997**, *12*, 185.
[35] H. Hähl, F. Evers, S. Grandthyll, M. Paulus, C. Sternemann, P. Loskill, M. Lessel, A. K. Hüsecken, T. Brenner, M. Tolan, K. Jacobs, *Langmuir* **2012**, *28*, 7747.
[36] J. M. Anderson, in *Principles of Regenerative Medicine (Second edition)*, (Eds: A. Atala, R. Lanza, J. A. Thomson, R. Nerem), Academic Press, San Diego, **2011**, 693.
[37] M. Wasilewska, Z. Adamczyk, B. Jachimska, *Langmuir* **2009**, *25*, 3698.
[38] R. F. Doolittle, *Annu. Rev. Biochem.* **1984**, *53*, 195.
[39] F. Putnam, Ed. *The Plasma Proteins: Structure, Function, and Genetic Control*, Elsevier, Amsterdam/New York, **1984**.
[40] a) R. A. Weinstein, R. Gaynes, J. R. Edwards, N. N. I. S. System, *Clin. Infect. Dis.* **2005**, *41*, 848; b) W. Ziebuhr, S. Hennig, M. Eckart, H. Kränzler, C. Batzilla, S. Kozitskaya, *Int. J. Antimicrob. Agents* **2006**, *28*, 14; c) G. E. Pierce, *J. Ind. Microbiol. Biotechnol.* **2005**, *32*, 309.
[41] P. Kingshott, J. Wei, D. Bagge-Ravn, N. Gadegaard, L. Gram, *Langmuir* **2003**, *19*, 6912.
[42] A. Lau, 2050, Accurate long.
[43] J. Kuang, P. B. Messersmith, *Langmuir* **2012**, *28*, 7258.
[44] J. Pei, H. Hall, N. D. Spencer, *Biomaterials* **2011**, *32*, 8968.
[45] E. A. Cavalcanti-Adam, T. Volberg, A. Micoulet, H. Kessler, B. Geiger, J. P. Spatz, *Biophys. J.* **2007**, *92*, 2964.
[46] H. J. Busscher, H. C. van der Mei, G. Subbiahdoss, P. C. Jutte, J. van den Dungen, S. A. J. Zaat, M. J. Schultz, D. W. Grainger, *Sci. Transl. Med.* **2012**, *4*, 153rv10.
[47] Â. Serrano, O. Sterner, S. Mieszkin, S. Zürcher, S. Tosatti, M. E. Callow, J. A. Callow, N. D. Spencer, *Adv. Funct. Mater.* **2013**, *23*, 5706.
[48] a) T. Morisaku, J. Watanabe, T. Konno, M. Takai, K. Ishihara, *Polymer* **2008**, *49*, 4652; b) K. Ishihara, H. Nomura, T. Mihara, K. Kurita, Y. Iwasaki, N. Nakabayashi, *J. Biomed. Mater. Res.* **1998**, *39*, 323.
[49] T. Moro, Y. Takatori, K. Ishihara, T. Konno, Y. Takigawa, T. Matsushita, U. I. Chung, K. Nakamura, H. Kawaguchi, *Nat. Mater.* **2004**, *3*, 829.